Research Article

Unpolarized Raman Spectra Shift in Solidified Oil-Water-Saltwater

Saddam Husain Dhobi *, Surendra Hangsarumba, Kishori Yadav, Suresh Prasad Gupta

Department of Physics, Patan Multiple Campus, Tribhuvan University, Patandhoka, Lalitpur-44700, Nepal

***Corresponding authors** *:* saddam@ran.edu.np
https://doi.org/10.55674/ias.v14i2.251839

Received: 05 March 2023; **Revised:** 08 March 2025; **Accepted:** 12 March 2025 ; **Available online:** 1 May 2025

Abstract

The study of unpolarized Raman spectral shifts in solidified oil-water-saltwater systems is crucial for understanding complex multiphase interactions under varying environmental conditions. Such systems are commonly found in natural and industrial processes, including oil spill remediation, geological formations, and desalination technologies. The need for detailed insights into molecular behavior and structural changes during solidification arises from the necessity to optimize these processes and mitigate environmental impacts. By analyzing Raman spectral shifts, this research provides essential information on the reorganization of molecular bonds and the influence of saltwater on oil-water interfaces, contributing significantly to environmental science, materials engineering, and energy resource management. The objective of this study is to analyze the transmittance, absorbance, and Raman shift spectra of water, soybean oil, and saltwater using an unpolarized visible spectrum at a low temperature of –10 °C. Experimental observations indicate that transmittance decreases with increasing wavelength, while absorbance increases. The transmittance and absorbance behaviors exhibit a nonlinear (bumping) pattern due to molecular rotational and vibrational effects. Additionally, intensity ratio analysis before and after the increase reveals two Gaussian peaks: one between 2×10^3 cm^{-1} and 4×10^3 cm^{-1} and another between 5×10^3 cm^{-1} and 8×10^3 cm^{-1} for water, soybean oil, and saltwater. The intensity ratio for water and the water-soybean oil-saltwater sample is higher when observed with Raman spectral shifts. This is due to the high polarizability of the molecules caused by molecular vibrations and dipole moments. At the considered temperature, in terms of transmittance, soybean oil exhibits the highest transmittance at higher wavelengths, making it the most efficient for light transmission. In contrast, saltwater has the highest absorbance at high wavelengths, meaning it absorbs more light compared to water and soybean oil.

Keywords*:* Titanium dioxide; Silver doping concentration; Sol-gel and precipitation methods; Morphological and chemical analyses; Simple regression analysis.

1. Introduction

Edible oils are complex mixtures of organic substances that hold significant commercial value in industries such as food, pharmaceuticals, perfumes, and cosmetics due to their biological properties. Some optical properties of edible oils used in Sudan were measured using UV-VIS spectroscopy (190 – 1100 nm). The results, as reported by Banaga et al. [1], showed an increase in transmittance with the rising wavelength of visible light. The absorption index of all nine edible oil brands decreased with increasing temperature in the spectral range from 500 – 1100 nm. The absorption peaks observed in all the studied edible oils are attributed to the overtones and combinations of C–H stretching vibrations from various chemical groups (–CH2, –CH3, –CH, CH–) [2]. The unpolarized Raman spectra of solidified oil-water-saltwater systems provide significant insights into molecular interactions and phase transitions. Analyzing these spectra helps identify vibrational modes of the components, which is essential for understanding their behavior under different conditions. Raman spectroscopy is a powerful tool for detecting phase transitions in oil-water-saltwater mixtures by examining vibrational spectra at varying pressures and temperatures [3]. The presence of salts alters the vibrational modes of water, notably shifting the O-H stretching vibrations,

which can be quantitatively analyzed to determine salt concentration and type [4]. Low-frequency Raman spectra indicate that temperature affects the translational and rotational modes of water, influencing the overall spectral profile [5]. Additionally, salt modifies the hydrogen-bonding network in water, producing distinct spectral features linked to salinity levels [6 – 7].

The change in intensity when light passes from pure water and seawater ranges from order $10^{-4} – 10^{-3}$ with in optical paths from 25 – 100 cm experimentally, as reported by Lee et al. [8]. The total absorption coefficient exhibits a flat minimum around 410 – 420 nm, about twice that of pure water. At 310 nm, the total absorption coefficient may be as low that is half the value generally accepted for pure water [9]. The primary wavelength-dependent parameters that determine the widely varying pool colors are the reflectance of the rocks or the microbial mats growing on the rocks beneath the water and optical absorption and scattering in the water. The nature of absorbance coefficient determined by Shaw shows that the absorbance coefficient increases with the wavelength of light [10].

The dielectric properties of polar liquids, focusing on a water model with short-range intermolecular interactions using local molecular-field theory. The model effectively captures key dielectric properties and is a valuable tool for understanding solvation behavior and modeling confined fluids [6]. Strong hydrogen bonding in liquid water reduces structural heterogeneity, while time-resolved infrared and sum-frequency generation spectroscopy show that vibrational relaxation time increases with OH stretching frequency, ranging from 250 – 550 fs in bulk water, with even stronger frequency dependence at the air/water interface, confirming structural heterogeneity in liquid water [11]. Studies on seawater extinction show that filtering methods can distinguish between particle and dissolved matter absorption, although this is labor-intensive for routine work. Transparency measurements help identify water masses and assess absorption by particles and yellow substances [12]. The absorption cross-section of KCl vapor was used to derive absorption curves for NaCl, NaOH, and KOH, with no significant spectral changes observed across temperatures [13]. Raman spectroscopy, though limited by low scattering, is being explored for studying thermally stressed edible oils by correlating it with optical transmission and iodine value measurements [14]. The refractive indices of various oils were accurately characterized using the Cauchy eq. [15].

Water's absorption is influenced by rotational and vibrational modes, and its density variations, due to ions and temperature, affect absorption. Studies have shown that pure and saltwater reduce material stiffness and yield stress but have little effect on strain rate sensitivity and tensile ductility [16 – 17]. Water's conductivity differs significantly from seawater due to dissolved salts, affecting absorption at long wavelengths [18]. Correlations between salinity and absorbance allow for the identification and concentration estimation of salt solutions with minimal error [19]. Salinity impacts oceanography, evaporation, precipitation, and marine life distribution, influencing biological research, climate simulations, and weather forecasting [20 – 22]. Raman spectra of seawater, affected by temperature and salinity, show small variations, and Raman spectroscopy has been used to study these effects at constant temperatures [23].

Vibrational relaxation in water is influenced by molecular motion, and ions affect water's molecular structure, causing spectral differences between pure water and seawater [24, 25]. Raman spectroscopy also distinguishes liquid from hydrate phases and identifies chemicals without contact [26], particularly useful in geochemical mineral identification [27]. Temperature-induced changes in Raman spectra, such as OH stretching, are useful for temperature estimation [28]. The novelty of this work is to study the absorbance and transmittance because the fact that boundary interaction of light with molecules is one of the interesting properties of material and has wide rages of applications and an active research field. The absorption spectra can be studied by different techniques but the principle is same. The transmittance and absorbance principle are used to study chromophores present in the tissue, tissue oxygenation and total haemoglobin, no a specified vegetable oil for the component analysis of the female breast tissue, whereas others have used olive oil, raw pig lard, sunflower oil, or soybean oil, etc.

2. Materials and Methods

The electrostatic potential distribution on a molecule's van der Waals surface reflects variations in charge density and electrostatic interactions, which influence the molecule's reactivity and solvent behavior. A typical approach for predicting electrophilic and nucleophilic reaction sites is to examine this electrostatic potential distribution on the molecule's van der Waals surface. The relevant description is provided by;

$$V_{tot}(r) = V_{nuc}(r) + V_{ele}(r) = \sum_A \frac{Z_A}{r-R_A} \int \frac{\rho(r')}{r-r'} dr' \quad (1)$$

Where Z is the atom's nuclear charge, A is the nucleus coordinate, and R is the nucleus coordinate, and ρ is the electron density. The electrostatic potential has two components, as can be shown from eq. (1): nuclear charge and electron density [29]. The principal-axis components of the polarizability tensor in eq. (1) are represented as for different quantum mechanics systems as;

$$\alpha_{ii} = \frac{4\mu q^2 C_i L_i^4}{\hbar^2} \tag{2}$$

Where C_i is a constant whose value is determined by the properties of a quantum particle with mass is μ and charge is q. The characteristic length L_i is a measurement of the spatial spread of the groundstate wave function (Ψ_0) with regard to its center of mass $R = (R_1, R_2; \ldots, R_N) = \langle \Psi_0 | \hat{r} | \Psi_0 \rangle 0 | r | 0 >$, which in the case of atoms corresponds to the nuclear position. For a QM system represented by its ground-state wave function, the Euclidean L2 norm of the position vector, (r -R), is defined as;

$$L_i = \sqrt{\int (\boldsymbol{r_i} - \boldsymbol{R_i})^2 |\Psi_0(\boldsymbol{r})|^2 d\boldsymbol{r}^N} \tag{3}$$

Where N is the spatial dimensionality of the system**.** QM systems of any dimensionality since eq. (2) connects ii with the characteristic length L_i along the i^{th} principal axis**.** The generalization of eq. (2) to a many-particle system. By applying eq. (2) to each electron shell, we study many-electron atoms. The (isotropic) atomic polarizability in this situation reads;

$$\alpha = \frac{4m_e e^2}{\hbar^2} \sum_k^{occ} \frac{C_k}{\eta_k} \frac{L_k^4}{N_k} \approx \tilde{C} \left(\frac{4m_e e^2}{\hbar^2} \right) \sum_k^{occ} \frac{L_k^4}{\eta_k N_k} \tag{4}$$

L_k is obtained by eq. (3) for the kth orbital, and N_k is its occupation number derived from the many-electron version, where the sum runs over occupied orbitals with degenerate orbitals treated together, L_k is obtained by eq. (3) for the kth orbital, and N_k is its occupation number derived from the many-electron version. Using the Tkatchenko-Scheffler (TS) method, compute the polarizabilities of 1641 small organic compounds using eq. (2). Because of the direct relationship between atomic volume and polarizability, molecule polarizabilities in the TS technique are approximated by a sum of effective atomic polarizabilities stated in terms of free atom polarizabilities.

$$\alpha_{mol}^{TS} = \sum_n \alpha_n^{eff} = \sum_n \alpha_n^{eff} \left(\frac{V_n^{eff}}{V_n^{free}} \right) \tag{5}$$

Where the total is applied to all of the atoms in the molecule The Hirschfeld partitioning of the electron density yields the weights $\left(\frac{V_n^{eff}}{V_n^{free}} \right)$ that measure the volume ratio of an atom in a molecule to a free atom in vacuum. Eq. (5) is modified as follows based on the relationship of eq. (2) as;

$$\alpha_{mol}^{TS} = \sum_n \alpha_n^{eff} = \sum_n \alpha_n^{eff} \left(\frac{L_n^{eff}}{L_n^{free}} \right)^4 \tag{6}$$

Intermolecular interactions, spectroscopic observables, and vacuum polarization are all affected by polarizability, which is a critical response attribute of physical and chemical systems. The physical interpretation of polarization mechanisms is complicated by an infinite sum over all excited (bound and continuum) states when calculating the polarizability for quantum systems [30]. This makes the design of efficient response models more difficult. The Lambert-Beer law forms the foundation of UV-Vis spectroscopy-based quantitative studies of water quality parameters. The Lambert-Beer law relies on a monochromatic parallel laser beam irradiating the surface of the tested medium for measurement [31]. After passing through a medium of specific thickness, a portion of the light energy is absorbed by the medium, reducing the intensity of the transmitted light that passes through it as shown in Fig 1. The thickness of the absorption medium has a direct relationship with its absorbance.

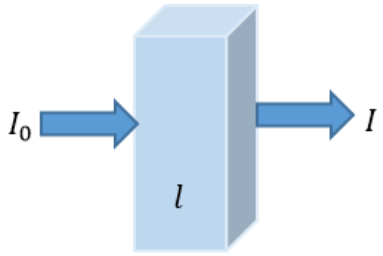

Fig.1 Schematic diagram of the Lambert-Beer law.

Mathematical expression of the Lambert-Beer law is as follows;

$$A = \log\left(\frac{1}{T}\right) = Kal \tag{7}$$

Where A is the absorbance, T is the transmittance, defined as the ratio of the intensity of the outgoing light (I) to the intensity of the incident light (I_0); K is the molar absorption coefficient, which is related to the nature of the absorbing substance and the wavelength (λ) of the incident light; a is the concentration of the absorbing substance in mol L^{-1}; and l is the thickness of the absorbing layer in cm [32]. The reflectivity spectrum was calculated from the absorption and transmittance spectra according to the law of energy conservation [1].

$$R(\text{Reflectivity}) = 1 - \sqrt{Texp(A)} \tag{8}$$

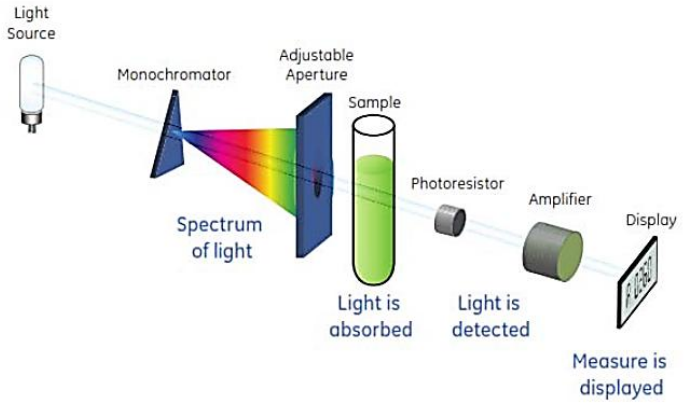

Fig. 2 Experimental diagram of spectrophotometer to measure transmittance.

Iron **(**III**)** nitrate nonahydrate ($Fe(NO_3)_3(H_2O)_9$, Sigma-Aldrich), lithium phosphate monobasic (LiH_2PO_4, Sigma-Aldrich), Polyacrylonitrile ($(C_3H_3N)_n$ Sigma-Aldrich), N, N-dimethylformamide anhydrous ($HCON(CH_3)_2$, SIAL), and polyethylene glycol ($H(OCH_2CH_2)$Noh, Sigma-Aldrich**)** were used as the precursor substances for preparing the composite materials. Carbon black (C, Alfa Aesar) polyvinylidene difluoride ($(CH_2CF_2)_n$, Sigma-Aldrich), and 1-Methyl-2pyrolidinone (C_5H_9NO, Sigma-Aldrich) were used as the substance for working electrode preparation. Potassium hydroxide (KOH, Sigma-Aldrich) was used as the electrolyte in a three-electrode testing system. Lithium hexafluorophosphate solution was used as an electrolyte in coin cells.

2.1 Sample Preparation

First, saltwater was prepared by dissolving 3 g of NaCl into 150 mL of drinking water. For this study, three different solid cubes were prepared: water, oil, and saltwater, to examine their transmission, absorption, and reflection properties. Additionally, a solid cube with three layers of different liquids (water = 1.50 cm, oil = 0.50 cm, and saltwater = 2 cm) was created by solidifying the layers one by one, in the following order: water to soybean oil to saltwater, oil to water, and saltwater to water to soybean oil. These layered cubes were prepared to study the boundary transmittance properties**.** For example, the soybean oil-saltwater-water cube was prepared by first placing the soybean oil in the cube mold and freezing it for 30 min at

–10 °C**.** After the oil solidified, saltwater was added to the surface of the formed cube and frozen for another 30 min. at –10 °C, forming a solid saltwater layer. Finally, water was added to the surface of the saltwater layer and left to freeze for 30 min at –10 °C. Once the cube was formed, its properties were tested using a Thermino spectrometer, as shown in Fig. 2.

3. Results and Discussions

3.1 Comparison of Transmittance Properties of the Soybean oil, Water, and Saltwater

Fig. 3 below represents the variation in the transmittance properties of oil, water, and saltwater with wavelength at −10 °C. The observations show that transmittance ranges from 20 – 98.50%. The transmittance as a function of wavelength follows a nonlinear pattern for soybean oil, water, and saltwater. This nonlinear nature is due to molecular vibrations and bond stretching. At the specific wavelength of 617.10 nm, the transmittance values observed for soybean oil, water, and saltwater were 62.90%, 61.60%, and 54.40%, respectively. The maximum transmittance was observed at 454.50 nm for saltwater and 553.20 nm for water. In the lower wavelength region, the transmittance of saltwater is higher, while at higher wavelengths, the transmittance is lower compared to soybean oil and water. This difference is attributed to the ionization of sodium chloride present in the sample. Due to ionization, the interaction of the spectrum with sodium and chloride ions is minimal, while such phenomena are not observed in the other two samples, water and oil. At considered temperature, in terms of transmittance, soybean oil has the highest transmittance at high wavelengths, making it the best for light transmission.

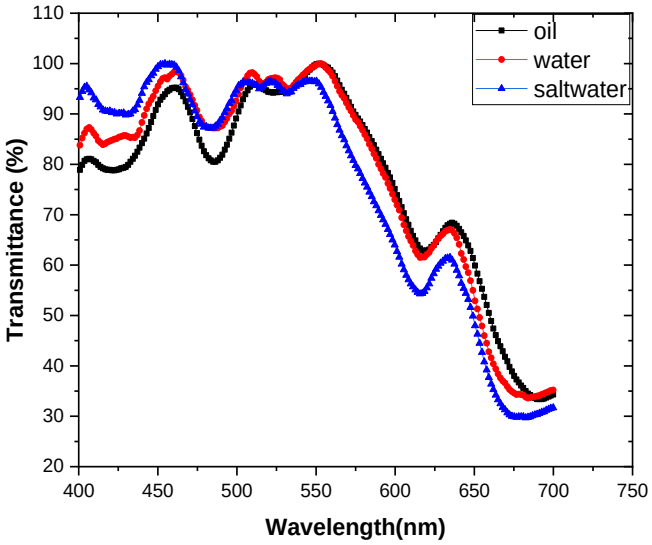

Fig. 3 Transmittance properties of the soybean oil, water, and saltwater**.**

3.2 Comparison of transmittance properties of the soybean oil, water, and saltwater

Fig. 4 below represents the variation in the absorbance properties of oil, water, and saltwater with wavelength. The absorbance of light ranges from 0 – 0.55 a.u. At the same wavelength of 634.60 nm, the absorbance values for oil, water, and saltwater are 0.17 a.u., 0.17 a.u., and 0.21 a.u., respectively. The absorbance properties of oil, water, and saltwater increase with the increase in wavelength. Saltwater shows minimal absorption at low wavelengths and higher absorption at high wavelengths, while water's absorbance lies between that of oil and saltwater. In terms of absorbance, saltwater exhibits the highest absorption at high wavelengths, meaning it absorbs more light compared to water and soybean oil at the considered temperature.

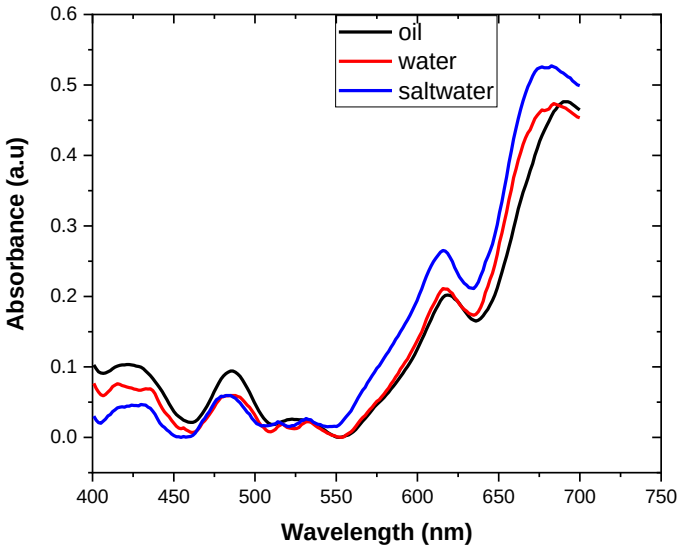

Fig. 4 Absorbance properties of the soybean oil, water, and saltwater**.**

3.3 Cross-Correlation of Transmittance of Water With Saltwater and Soybean Oil

Fig. 5 below represents the correlation between water, saltwater, and oil, respectively. The observation shows a strong correlation, indicating that there is a significant relationship between water and both saltwater and oil.

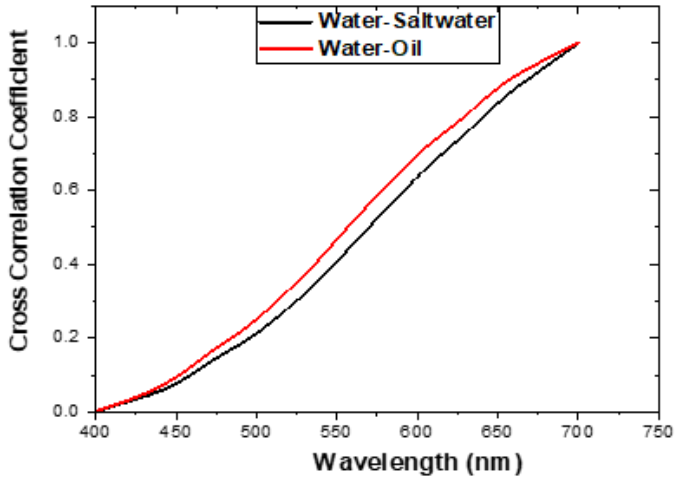

Fig. 5 Cross-Correlation of transmittance properties of water with salt water and oil.

3.4 Raman Shift for oil, water and saltwater at −10 °C

In the soybean oil sample, the observed intensity ratio shows a lower minimum at lower Raman spectral shifts and a higher ratio at higher wavelengths compared to saltwater and water. The intensity ratio of saltwater is high at low Raman spectral shifts and low at higher shifts, in comparison to oil and water. All samples show two Gaussian peaks, one between 2 × 10^3 cm^{-1} and 4 × 10^3 cm^{-1} and another between 4 × 10^3 cm^{-1} and 8 × 10^3 cm^{-1}. The intensity ratio is higher at certain Raman spectral shifts because when the incident spectrum interacts with the molecules, the energy is transferred to the molecules, causing them to vibrate. This vibration induces a dipole moment, and molecular bonds stretch, which results in polarization of the molecules. The Gaussian peaks observed are due to the polarization of molecules and the resonance, as shown in Fig. 6.

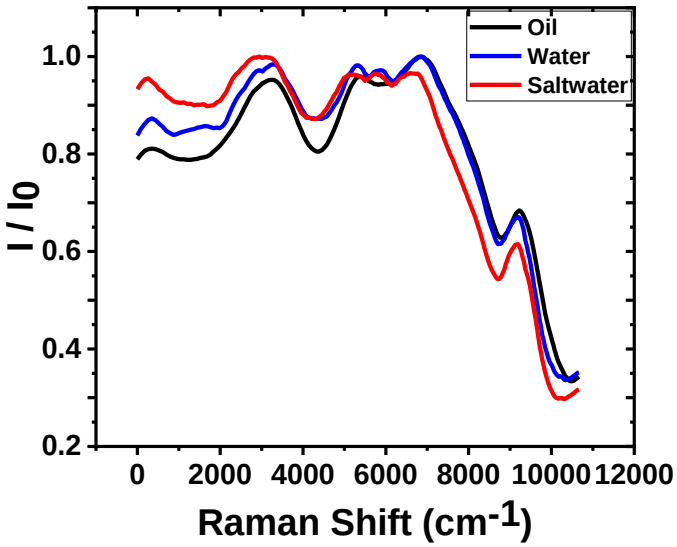

Fig. 6 Comparison of Raman shift of the Oil, water, and saltwater.

The nature of Raman spectra shifting with statistical analysis is shown in Fig. 7. The Raman shifts of saltwater at different concentrations, observed by Bao et al. between $3\times 10^3 - 3.80 \times 10^3$ cm^{31}, is similar to the present work, as shown in Fig. 6 [33]. Additionally, the Raman spectra of the OH-stretching vibration of liquid water from $MgCl_2$/water exhibit a similar pattern to our observations between $3\times 10^3 - 38 \times 10^3$ cm^{-1}. The interaction of salt ions and water is governed by Coulombic forces, which are much stronger than the interaction between two water molecules that interact via hydrogen bonds. The Raman shift of the OH-stretching vibration of water from the liquid water-rich phase also exhibits a similar pattern to our observation between $3\times 10^3 - 38 \times 10^3$ cm^{-1} [34].

The fitted equation is polynomial equation of 9 deg., the fitted equation for oil is represent by y_0, water is y_W and saltwater is y_{SW}. Eq. (9) represent the polynomial fitted equation of oil with Adj. R-Sqr = 0.98, maximum standard error 2.28% for 73.22 intercept and minimum tends to zero for 3.37×10^{-1} as,

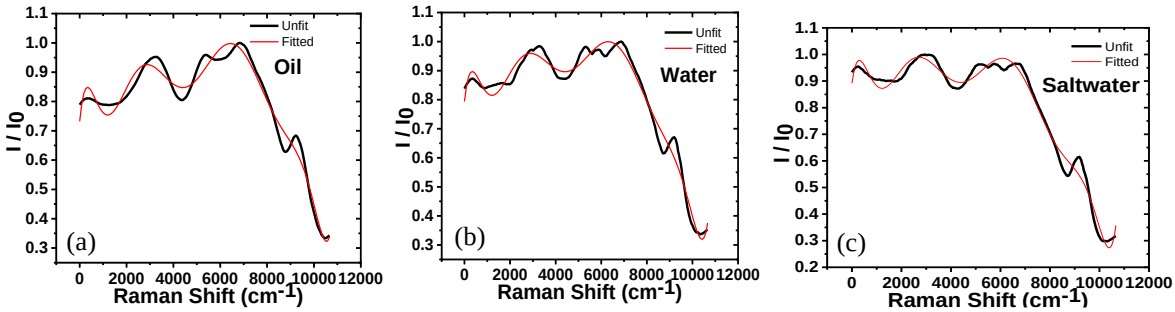

Fig. 7 Ratio of intensity of transmitted and incident light versus Raman shift (a) oil, (b) water and (c) saltwater.

$$y_0 = 73.22 + 0.09x - 2.07 \times 10^{-4}\,x^2 + 1.96 \times 10^{-7}\,x^3 - 9.23 \times 10^{-11}x^4 + 2.45 \times 10^{-14}x^5 - 3.77 \times 10^{-18}x^6 + 3.41 \times 10^{-22}x^7 - 1.66 \times 10^{-26}x^8 + 3.37 \times 10^{-31}x^9 \quad (9)$$

Eq. (10) represents the polynomial fitted equation of water with Adj. R-Sqr = 0.98, with maximum standard error 2.23% for 79.38 intercept and minimum tends to zero for 3.01×10^{-31} as,

$$y_w = 79.39 + 0.08x - 1.80 \times 10^{-4}\,x^2 + 1.70 \times 10^{-7}\,x^3 - 8.00 \times 10^{-11}x^4 + 2.12 \times 10^{-14}x^5 - 3.30 \times 10^{-18}x^6 + 2.99 \times 10^{-22}x^7 - 1.47 \times 10^{-26}x^8 + 3.01 \times 10^{-31}x^9 \quad (10)$$

Eq. (11) represents the polynomial fitted equation of saltwater with Adj. R-Sqr = 0.99, with maximum standard error 2.13% for 79.38 intercept and minimum tends to zero for 3.62×10^{-31} as,

$$y_{sw} = 89.17 + 0.07x - 1.85 \times 10^{-4}\, x^2 + 1.82 \times 10^{-7}\, x^3 - 8.82 \times 10^{-11} x^4 + 2.39 \times 10^{-14} x^5 - 3.80 \times 10^{-18} x^6 + 3.52 \times 10^{-22} x^7 - 1.75 \times 10^{-26} x^8 + 3.62 \times 10^{-31} x^9 \quad (11)$$

3.5 Raman Shifting at Interface Boundary Layer

The Fig. 8 below, depicts the relationship between Raman spectra shift with intensity ratio of sample which contain three materials (water, saltwater and soybean oil) layer by layer with different arrangement like water-soybean oil-saltwater(W-O-S), soybean oil-saltwater-water (O-S-W) and saltwater-water-soybean oil (S-W-O). The observation shows that the intensity ratio is high at lower and high Raman spectra shift for saltwater-water-soybean oil. The Gaussian peak of sample with different materials layer by layer is similar to sample of water, soybean and saltwater. The intensity ratio with increasing the Raman spectra shift decrease.

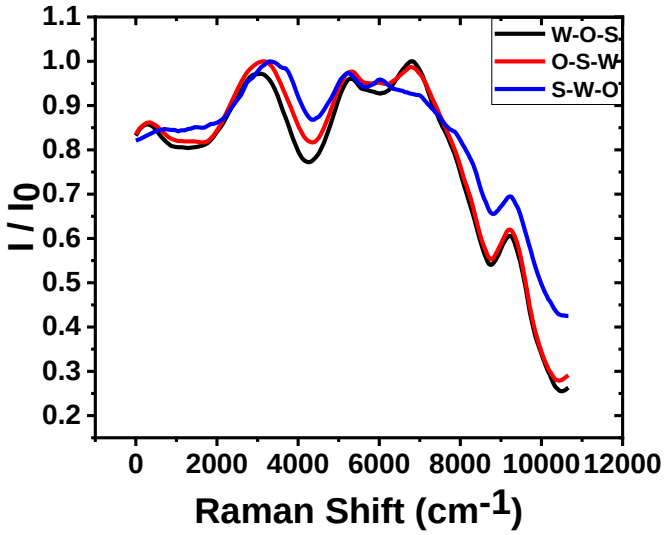

Fig. 8 Comparison between the I / I_0 and Raman shift.

The fitted polynomial for Raman spectra shifting for the sample of different three materials layer by layer at −10 °C is shown in Fig. 9. The observation shows intensity ratio shifted towards high Raman spectra and the Gaussians peak also decrease. This is because molecular vibration and bond stretch when spectrum in incidence on sample. In case of water-soybean oil-saltwater sample, the spectrum enter into in water layer and energy of spectrum get reduce and have not enough energy therefore the vibration for other layer molecules is low and the observed Gaussians peak is smooth with sharp peak. In case of soybean oil-saltwater-water sample, the energy loss in soybean oil is less and remain energy of spectrum also cause vibration to sodium ion and water molecules. Therefore, a constant intensity ratio is observed around 6×10^3 cm^{-1} and Gaussians peak become flatter with lower intensity ratio. In case of saltwater-water-soybean oil sample, the sodium ion presents in sample disturbed the sharpness of Gaussians peak because the incidence spectrum goes interact with sodium ions as well as water in first layer (saltwater) and remain energy caused low vibration for other layer of sample.

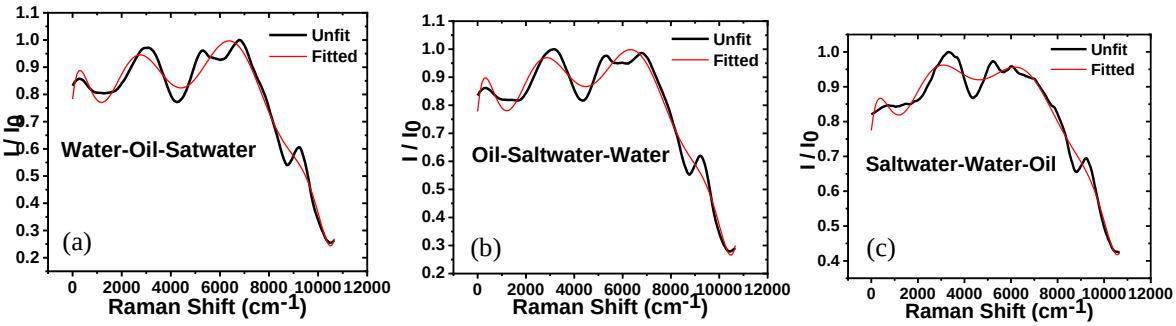

Fig. 9 The Raman shift of (a) water-oil-saltwater, (b) oil-saltwater-water, and (c) saltwater-water-oil.

The fitted equation is polynomial equation of 9 deg., the fitted equation for water-oil-saltwater boundary is represent by y_{wos}, oil-saltwater-water boundary is y_{wos} and saltwater-water-oil boundary is y_{wos}. eq. (12) represents the polynomial fitted equation of water-oil-saltwater with Adj.R-Sqr = 0.98, with maximum standard error 2.59% for 78.30 intercept and minimum tends to zero for 4.01×10^{-31} as;

$$y_{wos} = 78.31 + 0.09x - 2.23 \times 10^{-4}\,x^2 + 2.19 \times 10^{-7}\,x^3 - 1.05 \times 10^{-10}x^4 + 2.83 \times 10^{-14}x^5 - 4.42 \times 10^{-18}x^6 + 4.02 \times 10^{-22}x^7 - 1.97 \times 10^{-26}x^8 + 4.01 \times 10^{-31}x^9 \quad (12)$$

Eq. (13) represents the polynomial fitted equation of oil-saltwater-water with Adj. R-Sqr = 0.98, with maximum standard error 2.59% for 78.30 intercept and minimum tends to zero for 4.01×10^{-31} as;

$$y_{osw} = 77.79 + 0.09x - 2.31 \times 10^{-4}\,x^2 + 2.21 \times 10^{-7}\,x^3 - 1.05 \times 10^{-10}x^4 + 2.77 \times 10^{-14}x^5 - 4.29 \times 10^{-18}x^6 + 3.88 \times 10^{-22}x^7 - 1.89 \times 10^{-26}x^8 + 3.86 \times 10^{-31}x^9 \quad (13)$$

Eq. (14) represent the polynomial fitted equation of oil-saltwater-water with Adj. R-Sqr =0.98, with maximum standard error 1.81% for 77.46 intercept and minimum tends to zero for 2.01×10^{-31}as;

$$y_{swo} = 77.46 + 0.06x - 1.38 \times 10^{-4}\,x^2 + 1.26 \times 10^{-7}\,x^3 - 5.80 \times 10^{-11}x^4 + 1.50 \times 10^{-14}x^5 - 2.30 \times 10^{-18}x^6 + 2.05 \times 10^{-22}x^7 - 9.93 \times 10^{-27}x^8 + 2.01 \times 10^{-31}x^9 \quad (14)$$

3.6 Nature of Maximum and Minimum Transmittance of Oil, Water, and Saltwater at 422.60 nm, 461.80 nm, 553.20 nm, 636 nm and 698.40 nm Wavelength

Considering the maximum peaks and minimum deep valley points of transmittance for the three samples (water, saltwater, and soybean oil) at certain wavelengths, the nature of transmittance with wavelength is shown in Fig. 10. The maximum transmittance (peak) is 99.10% at 461.80 nm for the saltwater sample, 100% at 553.20 nm for the water sample, and 68.40% at 636 nm for the soybean oil sample. The minimum transmittance (deep valley) is 78.8% at 422.60 nm for the oil sample and 31.60% at 698.40 nm for the saltwater sample.

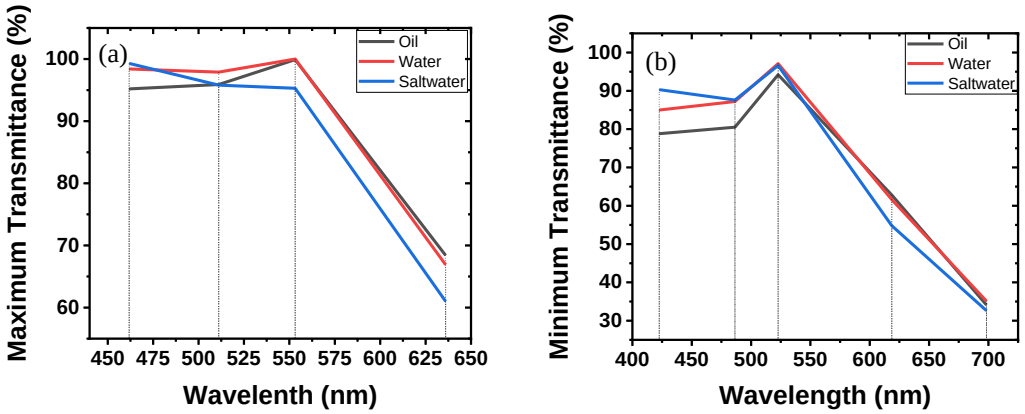

Fig. 10 The (a) maximum transmittance and (b) minimum transmittance of oil, water, and saltwater at fixed wavelength.

3.7 Refractive index of water, saltwater and oil with transmittance

The Fig. 11 shows a relation of refractive index and transmittance at wavelength of 589 nm. The oil has a greater value of transmittance of 82%, water has 80%, and saltwater has 70.80%. Oil has high refractive index with high transmittance whereas saltwater has minimum transmittance.

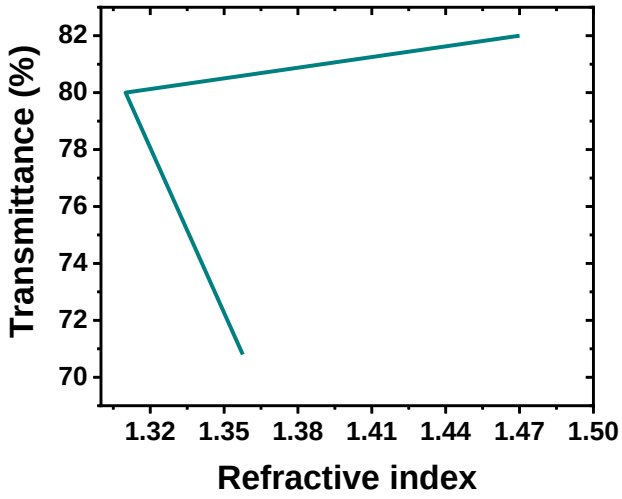

Fig. 11 The refractive index versus transmittance of soybean oil, water, salt water.

4. Conclusion

The transmittance properties of water, saltwater, and oil decrease as the wavelength increases, while absorbance exhibits the opposite trend. At the considered temperature, soybean oil demonstrates the highest transmittance at longer wavelengths, likely due to its molecular structure, which minimizes scattering and absorption. Saltwater shows the highest absorbance, as the ionization of sodium chloride enhances light interaction, leading to greater absorption at higher wavelengths. The nonlinear transmittance behavior of all three liquids is influenced by molecular vibrations and bond stretching at low temperatures. Statistical analysis reveals a strong cross-correlation between the transmittance of water, saltwater, and oil. The transmittance and absorbance of water-oil-saltwater, oil-saltwater-water, and saltwater-water-oil samples closely resemble the boundaries of their individual components. The Raman shift of oil, water, and saltwater is found to be at its maximum, while the intensity ratio is at its minimum. The most significant Raman shift is observed in solidified cubes of water and water-oil-saltwater. A statistical analysis shows that a ninth-degree polynomial equation provides the best fit for the experimental data. These optical properties have significant applications in atmospheric science, where light interactions with frozen or supercooled water influence climate models and remote sensing. In biomedical optics, understanding the behavior of biological fluids at low temperatures aids in cryopreservation and imaging techniques. The findings also have implications for food preservation and processing, where optical properties play a role in assessing the quality of frozen liquids and oils. Additionally, the observed nonlinear optical behavior can contribute to advancements in optical sensors, photonics, and spectroscopy, particularly in the development of temperature-sensitive optical materials and devices. Future research should further investigate the effects of extreme temperatures on these properties, leading to enhanced applications in thermal imaging, environmental monitoring, and advanced material science.

Acknowledgements

The authors would like to express their sincere gratitude to all the faculty members of the Department of Physics, Patan Multiple Campus, Tribhuvan University, Nepal, for their unwavering support and for providing the necessary laboratory facilities during the course of this experiment. Their valuable guidance and assistance have contributed significantly to the success of this research. Additionally, we would like to thank our colleagues and all those who helped in various aspects of the study.

References

[1] M.M.D.A. Banaga, A. Awadelgied, N.A.A. Muslet, A.A. Mohamed, A.S. Hamed, Investigation of Natural Pigments and Optical Properties for Some Sudanese Edible Oils Using UV - VIS Spectroscopy Techniques, Am. J. Mod. Phys. 10(5) (2021) 111 − 114.

[2] X. C. Li, 1 J. M. Zhao, L. H. Liu, J. Y. Tan, Optical properties of edible oils within the spectral range from 300 to 2500 nm determined by double optical path length transmission method, Appl. Opt. 54(13) (2015) 3886 – 3893.

[3] J. A. Schouten, J. P. J. Michels, High pressure behaviour of the vibrational spectra of mixtures in the fluid phase and at the fluid-solid transition. Kluwer Academic Publishers, 1999.

[4] T. Kauffmann, I. Durickovic, P. Bourson, M. D. Fontana, M. Marchetti, R. Claverie, Capteur Optique Raman de Solutions Salines. In 12ème Congrès Francophone de Techniques Laser (CFTL 2010), (2010) 433 – 440.

[5] K. Winkler, J. Lindner, P. Vöhringer, Low-frequency depolarized Raman-spectral density of liquid water from femtosecond optical Kerr-effect measurements: Lineshape analysis of restricted translational modes, PCCP. 4(11) (2002) 2144 – 2155.

[6] C. Mao, Y. Chen, Y. Zhou, Y. Ge, Z. Zhou, Y.Z. Wang, Cryogenic Raman spectroscopic characteristics of NaCl-H2O, CaCl2-H2O and NaCl-CaCl2-H2O: application to analysis of fluid inclusions, Spectrosc. Spect. Anal. 30(12) (2010) 3258 – 3263.

[7] M. H. Brooker, M. Perrot, Raman light scattering studies of the depolarized low frequency region of water and aqueous solutions, *ChemInform. 12*(26) (1981).

[8] G. Wei, Z. Lee , X. Wu, X. Yu, S. Shang, R. Letelier, Impact of Temperature on Absorption Coefficient of Pure Seawater in the Blue Wavelengths Inferred from Satellite and In Situ Measurements, J. Remote Sens. 2021(9842702) (2021) 1 – 13.

[9] A. Morel, B. Gentili, H. Claustre, M. Babin, A. Bricaud, J. Ras, F. Tieche, Optical properties of the ‘‘clearest’’ natural waters, L&O. 52(1) (2007) 217 – 229.

[10] J. A. Shaw, P. W. Nugent, M. Vollmer, Colors of the Yellowstone thermal pools for teaching optics, in ETOP 2015 Proceedings, E. Cormier and L. Sarger, eds., Optica Publishing Group, 2015.

[11] S. T. Van der Post, C. S. Hsieh, M. Okuno, Y. Nagata, H. J. Bakker, M. Bonn, J. Hunger, Strong frequency dependence of vibrational relaxation in bulk and surface water reveals sub-picosecond structural heterogeneity. Nat. Commun. 6(1) (2015).

[12] N. G. Jerlov, Influence of Suspended and Dissolved Matter on the Transparency of Sea Water, Tellus. 5(1) (1953) 59 – 65,

[13] W. Weng, T. Leffler, C. Brackmann, , M. Alden, Z. Li, Spectrally Resolved UV Absorption CrossSections of Alkali Hydroxides and Chlorides Measured in Hot Flue Gases, Appl. Spectrosc.72(9) (2018) 1388 – 1395.

[14] H. Y. Lam, S. Ghosh, S. Chattopadhyay, Express: Calibrated Optical Markers to Study Thermal Degradation in Edible Oils Using Raman and Optical Transmission Spectroscopy, Appl. Spectrosc. (2019), 1 – 7.

[15] S. Xu, X. K. Li, Refractive index characteristics of edible oils based on spectrometry and erects of oil dispersion on OCT, *JIOHS.* 14(1) (2021) 1 – 4,

[16] R. Rottgers, D. McKee, Utschig, Temperature and salinity correction coefficients for light absorption by water in the visible to infrared spectral region, Opt. Express. 22(21) (2014) 25093 – 26000,

[17] G. Quino, A. Pellegrino, V. L. Tagarielli, N. Petrinic, Measurements of the effects of pure and salt water absorption on the rate-dependent response of an epoxy matrix, Compos B Eng. 146 (2018) 213 – 221,

[18] C.D. Mobley, Handbook of Optics: Optical Properties of Water, McGraw-Hill, Inc., (1994).

[19] R. D. Peters, S. D. Noble, Using near infrared measurements to evaluate NaCl and KCl in water, JNIRS. 27(2) (2019) 147 – 155.

[20] D. T. Phan, C. W. Jung, Multilayered salt water with high optical transparency for EMI shielding applications, Sci. Rep. 10(21549) (2020) 1 – 9.

[21] K. P. Helm, N. L. Bindoff, J. A. Church, Changes in the global hydrological-cycle inferred from ocean salinity, Geophys. Res. Lett. 37(18) (2010) 44222 – 44224.

[22] N. Xu, Z. Q. Liu, X. D. Zhang, Y. P. Xu, N. N. Luo, S. J. Li, J. J. Xu, X. D. He, J. L. Shi, Influence of temperature-salinity-depth structure of the upper-ocean on the frequency shift of Brillouin LiDAR, Opt. Express. 29(22) (2021) 36442 – 36444.

[23] J. S. Bartlett, K. J. Voss, S. Sathyendranath, A. Vodacek, Raman scattering by pure water and seawater, Opt. Express. 37(15) (1998) 3324 – 3330.

[24] L. Li, X. Zhang, Z. Luan, Z. Du, S. Xi, B. Wang, L. Cao, C. Lian, J. Yan, Raman vibrational spectral characteristics and quantitative analysis of H_2 up to 400°C and 40 MPa, J. Raman Spectrosc. 2018 1 – 10.

[25] K. C. Hester, S. N. White, E. T. Peltzer, P. G. Brewer, E. D. Sloan, Raman spectroscopic measurements of synthetic gas hydrates in the ocean, Mar. Chem. 98 (2006) 304 – 314.

[26] G. Mogilevsky, L. Borland, M. Brickhouse, A. W. Fountain III, Raman Spectroscopy for Homeland Security Applications, Int. J. Spectrosc. 2012 (808079) (2012) 1 – 12.

[27] T. M. DeCarlo, Characterizing coral skeleton mineralogy with Raman spectroscopy, Nat. Commun. 9(1) (2018) 5325.

[28] C. P. Artlett, H. M. Pask, Optical remote sensing of water temperature using Raman spectroscopy, Opt. Express. 23(25) (2015) 31844 – 31856

[29] X. Wu, D. Ren, Model of B9N9 Response under External Electric Field: Geometry, Electronic Properties, Reaction Activity, Molecules. 27(1714) (2022) 1 – 14.

[30] P. Szabo, S. Goger, J. Charry , M. R. Karimpour , D. V. Fedorov, A. Tkatchenko, Four-Dimensional Scaling of Dipole Polarizability in Quantum Systems, Phys. Rev. Lett. 128(070602) (2022) 1 – 7.

[31] Z. Jiang, K. Zhou, V.K. Sharma, Occurrence, transportation, monitoring and treatment of emerging micro-pollutants in waste water—A review from global views. Microchem. J. 110 (2013) 292 – 300.

[32] Y. Guo, C. Liu, R. Ye, Q. Duan, Advances on Water Quality Detection by UV-Vis Spectroscopy, Appl. Sci. 10(6874) (2020) 1 – 18,

[33] D. Bao, D. Hua, H. Qi, J. Wang, Investigation of a Raman scattering spectral model for seawater containing a composite salt solute, Opt. Express. 30(5) (2022) 6713 – 6725.

[34] C. C. Holzammer, A.S. Braeuer, Raman Spectroscopic Study of the Effect of Aqueous Salt Solutions on the Inhibition of Carbon Dioxide Gas Hydrates, J. Phys. Chem. B. 2019 (123) (2019) 2354 − 2361.